RSC Advances

PAPER

View Article Online
View Journal | View Issue

Cite this: *RSC Adv.*, 2023, **13**, 8409

Synthesis and characterization of silver nanoparticle embedded cellulose–gelatin based hybrid hydrogel and its utilization in dye degradation†

Saruchi, *[a] Vaneet Kumar,*[b] Diksha Bhatt,[b] Sadanand Pandey [c] and Ayman A. Ghfar[d]

The present work describes the synthesis of a cellulose and gelatin based hydrogel by the grafting of poly(acrylic acid) using ammonium persulphate (APS)-glutaraldehyde as the initiator–crosslinker system. The structure of the hydrogel was studied through scanning electron microscopy (SEM) and FTIR. The maximum swelling rate of C-G-g-poly(AA) was found to be 92 g g^{-1} at pH 10. The size and structure of the prepared silver nanoparticles (AgNPs) were studied through TEM and zeta potential, and it was found that the synthesized AgNPs were spherical and the size range was 11–30 nm. The reduction process followed pseudo 1st order kinetics. EtBr and eosin dye degradation were more than 4 times faster, when AgNPs were used with sodium borohydride. Thus, it can be concluded that the synthesized C-G-g-poly(AA) AgNPs hybrid hydrogel is effective for the reduction and degradation of carcinogenic dyes in wastewater.

Received 24th June 2022
Accepted 20th January 2023

DOI: 10.1039/d2ra03885d

rsc.li/rsc-advances

1. Introduction

The research on nanoparticles has contributed to material engineering, which increases its utilization in different sectors such as environment, industries, and medicine. The physical and chemical properties of nanoparticles are unique characteristics and are different from its bulk material.[1–3] The AgNPs have attracted attention in biomedicine, environment, and catalysis fields.[4–7] AgNPs are ecofriendly, cost and energy-efficient, and have been exploited as catalysts in many sectors. Fe_3O_4-graphene imbibed with SiO_2 nanocomposites was utilized as an efficient adsorbent for methylene blue dye. WS_2 quantum dots coupled to BiOCl nanosheets were used as a photocatalyst. Graphitic carbon nitride was utilized for the reduction and degradation of hexavalent chromium and sulfisoxazole.[8–11] Peroxymonosulfate and peroxydisulfate were used as photocatalytic fuel cell and also used for the degradation of reactive brilliant blue. Microspheres of dopamine and polydopamine were used for the treatment of water pollution and lead sequestration.[12–14] Nanocellulose acted as a support for the synthesis of different types of NPs. Cellulose nanocrystals acted as a support for the formation of silver and gold NPs through solvent-free reduction processes.[15–18]

Gelatin is a natural, biodegradable, and nontoxic animal protein having $-NH_2$ and –COOH functional groups. Gelatin can form hydrogels as they respond to temperature change, but they have poor physical and chemical stability which can be improved using another polysaccharide with better mechanical and chemical strength and thus lead to the formation of a hybrid hydrogel.[19–21] Cellulose is a plant polysaccharide and is biodegradable, ecofriendly, renewable, and a cheap resource present in nature. Various active hydroxyl groups are present in cellulose, which help in their chemical modification. It has the potential to stabilize silver nanoparticles.[22–24] Hydrogels are three-dimensional polymeric networks, which have the capacity to soak up plenty of water or biological fluid than their weight but remain insoluble in water.[25–28]

The hydrogels made up from two different types of natural polymers have better chemical and mechanical properties and have many applications.[29] Natural polysaccharides were modified by grafting with vinyl monomers and gave new prospects of its utilization in different sectors with better results. As per literature survey, the incorporation of gelatin in cellulose helps in improving the mechanical strength of the hydrogel.[30–32]

[a]*Department of Biotechnology, CT Institute of Pharmaceutical Sciences (CTIPS), CT Group of Institutions, Shahpur Campus Jalandhar, Punjab, India*

[b]*School of Natural Science, CT University, Ludhiana, Punjab, India. E-mail: vaneet2106@gmail.com*

[c]*Department of Chemistry, College of Natural Science, Yeungnam University, 280 Daehak-Ro, Gyeongsan, Gyeongbuk, 38541, Republic of Korea. E-mail: sadanand.au@gmail.com*

[d]*Department of Chemistry, College of Science, King Saud University, P. O. Box 2455, Riyadh 11451, Saudi Arabia*

† Electronic supplementary information (ESI) available. See DOI: https://doi.org/10.1039/d2ra03885d

The present work envisaged the synthesis of acrylic acid-grafted hybrid hydrogel of cellulose and gelatin with glutaraldehyde-APA as a crosslinker-initiator system. The porous network of the synthesized hydrogel was utilized for the preparation and stabilization of AgNPs. AgNPs-loaded synthesized hydrogel was employed as a catalyst for the removal of harmful dye.

AgNPs were formed by many precursors and reduction compounds. $AgNO_3$ reduced by CNC, $NaBH_4$, dopamine, ethylene glycol-PVP, and m-hydroxy benzaldehyde-SDS produced AgNPs in the size range of 10–50 nm, 14 nm, 15–20 nm, 50–115 nm, and 15–20 nm, respectively, but in the present work, AgNPs were formed in the size range of 11–30 nm. This depicted that the synthesized NPs were of better catalytic activity than the AgNPs synthesized in the literature because a smaller size of the nanoparticles means higher catalytic activity.[1,12,17,20,22]

2. Materials and methods

2.1. Materials

Cellulose, gelatin, silver nitrate ($AgNO_3$), acrylic acid (AA), APS, glutaraldehyde, sodium borohydride, sodium hydroxide, ethidium bromide (EtBr), and eosin were procured from Loba Chemie and were of analytical grade.

2.2. Synthesis of the hybrid hydrogel

A homogenous solution of cellulose was prepared by homogenizing cellulose in water, followed by the addition of gelatin with continuous stirring at 55 °C, followed by APS and 3 wt% glutaraldehyde. Then, acrylic acid was added dropwise. The prepared solution was then kept in a microwave for 3 min at 700 W for free radical polymerization. Microwave irradiation is used as compared to normal heating as it leads to the effective heating of the reactant in the solution. The polymerization and grafting reaction was faster in the presence of microwave irradiation. As the polymerization completed, C-G-g-poly(AA) was immersed in water to extract the copolymer and remove the homopolymer and unreacted monomers. The prepared hydrogel was then dried in a hot air oven at 50 °C.[33,34]

2.3. Swelling studies of C-G-g-poly(AA)

The swelling performance of C-G-g-poly(AA) was studied in DD water at 37 °C.[27] Dried C-G-g-poly(AA) (0.5 g) was kept in a flask having 100 mL DD water and incubated until constant weight was attained. The weight of the swelled hydrogel was taken. Percentage swelling (Ps) of the synthesized hydrogel was calculated using the given expression:[32,33]

$$\text{Percentage swelling (Ps)} = \frac{(W_s - W_d)}{W_d} \times 100$$

where, W_s and W_d are the weight of the swelled and dried hydrogel, respectively.

2.4. Synthesis of AgNPs-imbibed C-G-g-poly(AA)

1.0 g hydrogel was taken in a beaker having 10 mL H_2O. The pH was adjusted to 8–11 with 1 M NaOH. To the reaction flask, $AgNO_3$ solution was added dropwise with stirring. The prepared mixture was then heated at 100 °C for 4 min. As the heating progressed, the solution became brownish, which indicated the formation of nanoparticles of silver (AgNPs). Then, the mixture was incubated for 24 h so that silver nanoparticles could imbibe in the hydrogel matrix. Then, hydrogel-containing AgNPs were taken out and dried in a hot air oven so that constant weight could be obtained. Poly(acrylic acid) acted as a reducing agent in AgNPs synthesis.[34,35]

2.5. Degradation and reduction of dyes by AgNPs

The synthesized C-G-g-poly(AA)-AgNPs hybrid hydrogel was used for the catalytic reduction/degradation of the carcinogenic dyes ethidium bromide and eosin. Sodium borohydride (0.05 M) was taken in the flask having EtBr and eosin solution (0.001 M). 0.05 g of the synthesized C-G-g-poly(AA)-AgNPs was added to the solution. After mixing the solution thoroughly, the absorption of the spectrum was taken immediately a double beam UV-vis spectrophotometer. The UV-vis spectrum of the blank sample is also taken in the same condition.[36]

3. Results and discussion

Various physical and chemical interactions occurred in functional groups of cellulose, gelatin, glutaraldehyde, and acrylic acid molecules. The grafting of poly(AA) with cellulose and gelatin led to the synthesis of a three-dimensional network structure (Scheme 1). Ammonium persulphate, which acts as an initiator, produces free radical on cellulose and acrylic acid, which initiates the chain initiation process of copolymerization. The free radical present on acrylic acid undergoes grafting with cellulose and gelatin and propagates the reaction chain till there is a blocking of the reaction chains due to recombination and disproportionation between free radicals.

3.1. Swelling studies

The prepared hydrogel was studied for its swelling behavior as a function of time. The swelling capacity of a hydrogel depends on the interaction between diverse functional groups of polysaccharide and polymeric chains. pH also has a significant role in hydrogel swelling; thus, it was also studied. The results (Fig. 1a) demonstrated that pH has great influence on the swelling of the hydrogel. The swelling was higher in alkaline medium than the acidic medium. This can be explained on the basis that in acidic pH, there is intra/intermolecular hydrogen bonding between the –COOH groups, which leads to the shrinking of the hydrogel; thus, there is decrease in the swelling of the hydrogel.[37] The swelling rate was higher in alkaline medium due to the protonation of –COOH groups, which dissociate the secondary interactions. An increase in the swelling capacity may be due to the repulsion among carboxylate anions, which leads to the expansion of the hydrogel network, thus increasing the swelling capacity of the synthesized hydrogel. Fig. 1a and b depict that the maximum swelling ratio (92 g g^{-1}) was achieved at alkaline pH (10), and equilibrium was achieved after 3 h.

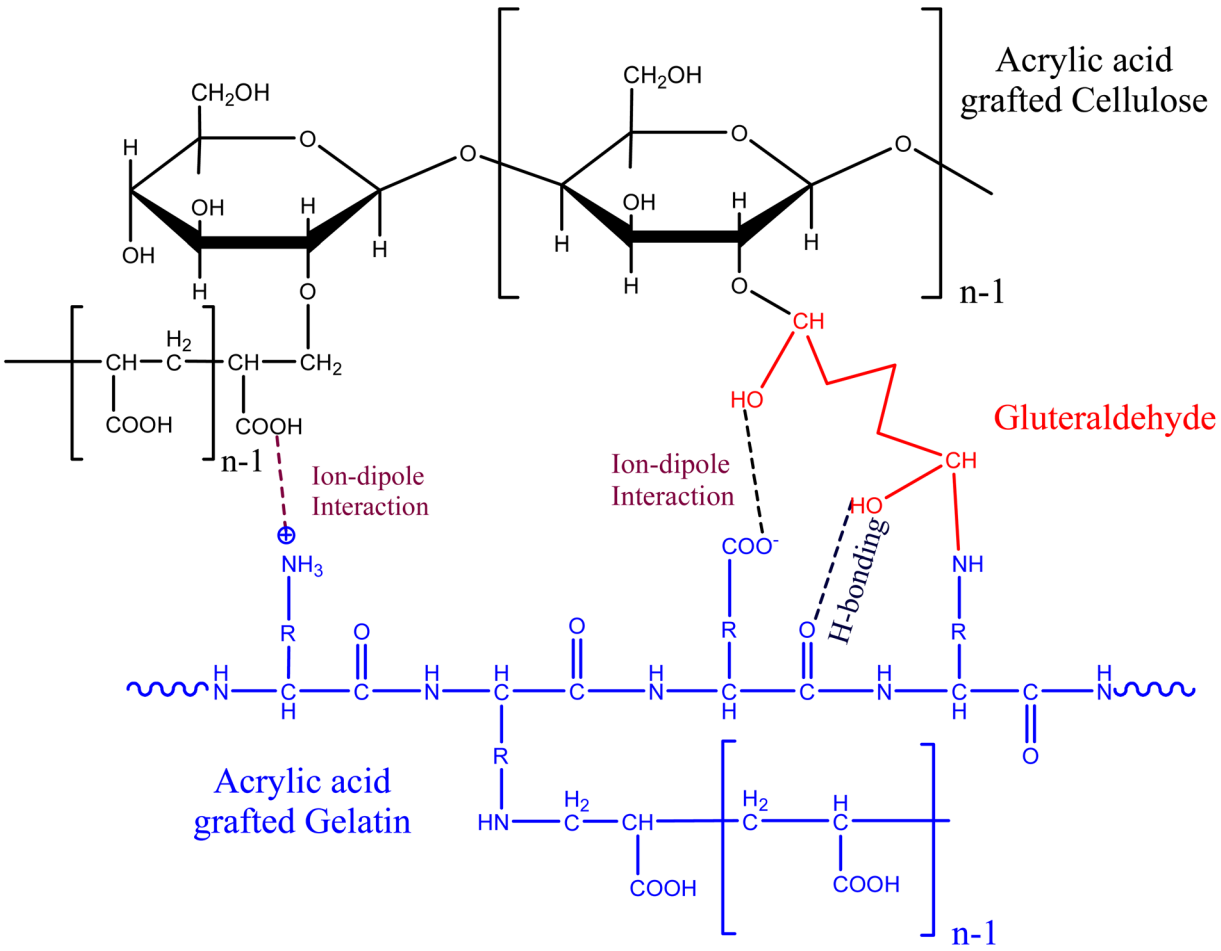

Scheme 1 Schematic diagram of crosslinked CG-g-Poly(AA).

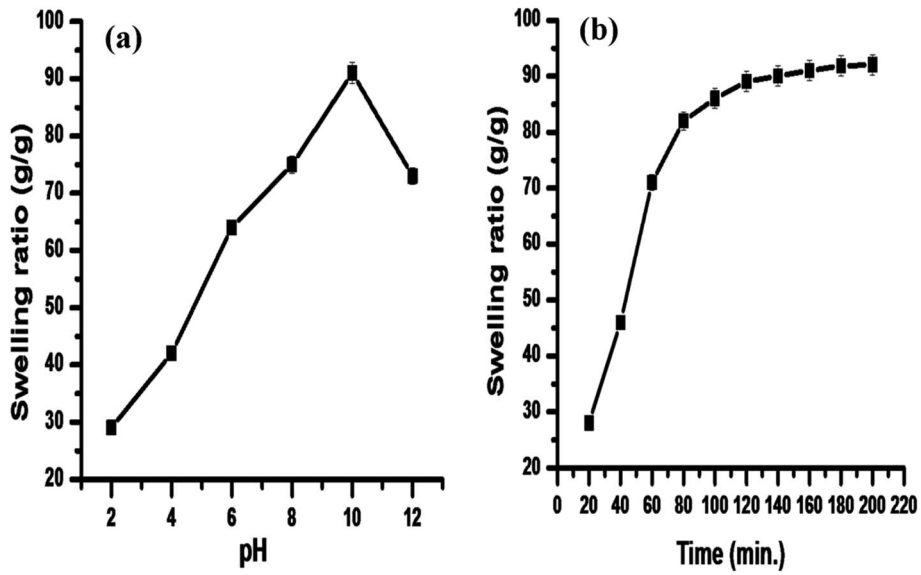

Fig. 1 Swelling ratio of the synthesized hydrogel at different (a) pH and (b) time.

3.2. Hydrogel characterization

3.2.1. FTIR. The FTIR spectrum of cellulose (Fig. 2a) has an absorption peak at 3150–3500 cm^{-1} due to the O–H group. The peak at 2800–2900 cm^{-1} is due to $-CH_2$ groups. Peaks at about 1400–1590 cm^{-1} occurred due to the $-COO^-$ groups. The peak at 1022 cm^{-1} is due to C–O–C. In case of gelatin, the absorption

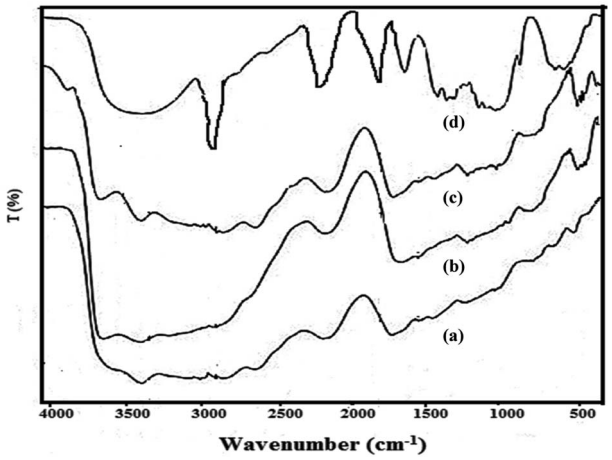

Fig. 2 FTIR spectra of (a) Cellulose; (b) Gelatin; (c) Cellulose–gelatin backbone; and (d) –C-G-g-poly(AA).

peaks at 3296 cm^{-1}, 1634 cm^{-1}, and 1245 cm^{-1} were due to the N–H stretching of amide-I, II, and III, respectively (Fig. 2b). The FTIR cellulose–gelatin hybrid backbone showed a shifting of peaks due to the presence of van der Waals interaction in both the backbones (Fig. 2c). The FTIR spectrum of CG-g-Poly(AA) (Fig. 2d) gave characteristic peaks of cellulose, gelatin, and acrylic acid. The grafted hydrogel showed peaks at 3400 cm^{-1} (cellulose), 1652 cm^{-1} (gelatin), and 1688 cm^{-1} (C=O stretching of acrylic acid), thereby confirming the grafting of poly(-acrylic acid) chains onto the hybrid backbone.[38,39]

3.2.2. SEM. The surface morphology of the backbones and C-G-g-poly(AA) was studied by the SEM technique (Fig. 3a–d). The SEM of cellulose showed networks with small blocks (Fig. 3a), while the SEM of gelatin showed networks of smooth rods (Fig. 3b). The hybrid backbone of cellulose–gelatin showed heterogenous morphology having blocks and rods in the structure (Fig. 3c). The SEM image of the hydrogel showed divergent morphology compared to the backbones. There is morphological variation in the synthesized hydrogel after grafting with acrylic acid and crosslinking with glutaraldehyde. A three-dimensional porous network of different size was observed in the SEM image of the synthesized hydrogel (Fig. 3d), which is a clear-cut indication of grafting.[40]

3.2.3. Mechanical properties. The restricted applications of the natural polymer were because of their weak mechanical strength, but it can be improved by the grafting of these naturally-occurring polymers. The compressive strength in the form of strain of the cellulose–gelatin backbone and the synthesized hydrogel are compared in Fig. 4. The synthesized

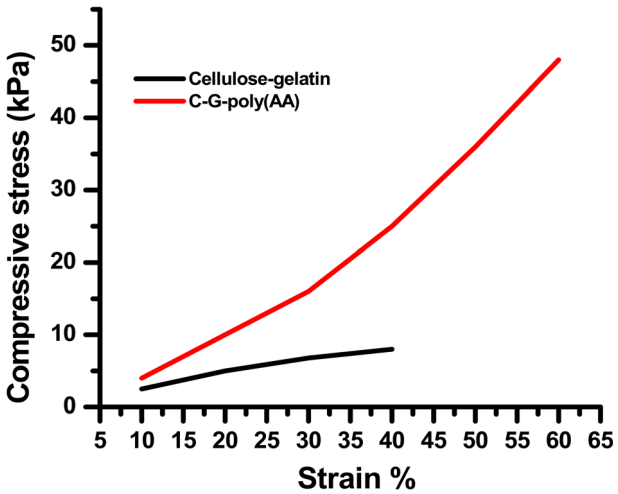

Fig. 4 Stress–strain curves of the cellulose–gelatin backbone and the synthesized hydrogel.

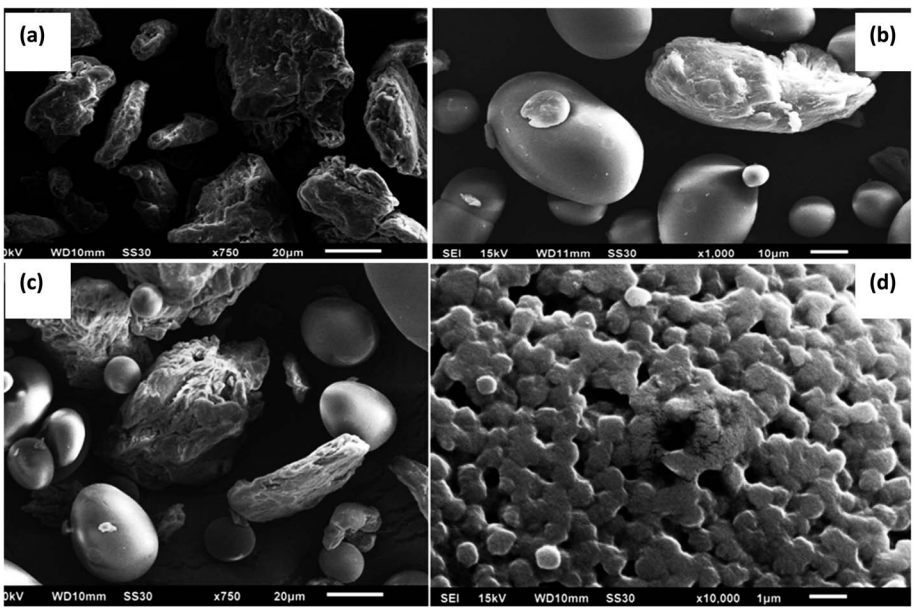

Fig. 3 SEM images of (a) Cellulose; (b) Gelatin; (c) Cellulose–gelatin hybrid backbone; (d) C-G-g-poly(AA).

hydrogel showed maximum compressive strain at 48 kPa, while the hybrid backbone showed the maximum compressive strain of 8 kPa. The results clearly indicated that the compressive strength of the prepared hydrogel was 6 times more than that of the hybrid backbone. The stress–strain relationship of the prepared hydrogel was initially found to be linear up to 30% of strain, but later on, it increased and attained maximum compression strength of 60% without collapsing, while the hybrid backbone collapsed at 40% strain. This clearly indicated that grafting and crosslinking enhanced the mechanical strength of the synthesized hydrogel.[41–43]

3.2.4. Thermal behavior. The thermal analysis of cellulose, gelatin, hybrid backbone, and synthesized hydrogel is given in Table S1.† Cellulose showed two-stage disintegration at 210.9–372.4 °C and 576.5–601.3 °C with weight loss of 28.2% and 65.3%, respectively. Gelatin showed only one stage decomposition at a temperature of 224.8–418.4 °C with 78% weight loss. The cellulose–gelatin hybrid backbone also showed two-stage disintegration at a temperature of 239.1–375.6 °C and 563.2–602.4 °C with weight loss of 58.4% and 38.1%, respectively. The TGA results clearly showed that grafting and crosslinking enhanced the thermal stability of the hydrogel. The TGA curve of the synthesized hydrogel showed three-stage decomposition in the temperature range of 260.3–300.4 °C, 372.6–512.8 °C, and 535.6–646 °C with weight loss of 21.6%, 52.3%, and 24.2%, respectively. The initial (262 °C) and final (644 °C) disintegration temperature of C-G-poly(AA) was higher than both the backbones. This clearly indicated that crosslinking and grafting increased the thermal stability of C-G-poly(AA).[43] DTA and DTG results also supported the TGA results. Exothermic peaks of DTA occurred at higher temperature than that of the backbones (Table S1†). The DTA peaks of the synthesized hydrogel also occurred at higher temperature (669 °C) than that of cellulose (596.5 °C), gelatin (312 °C), and the hybrid backbone (600.4 °C) (Table S1†).

3.2.5. XRD analysis. The nature of the backbones and synthesized hydrogel were studied through XRD. Cellulose showed a sharp peak ($2\theta = 20.25°$) (Fig. S1a†), which means that cellulose is crystalline in nature. The crystalline nature might be due to the intermolecular and intramolecular hydrogen bonding of the –OH and –COOH functional groups of the backbone.[43,44] The gelatin backbone showed a broad peak ($2\theta = 23.665°$), which indicated the amorphous nature of gelatin (Fig. S1b†).[20,43] The cellulose–gelatin hybrid backbone (Fig. S1c†) showed a peak with lesser intensity and crystallinity, which may be due to the presence of van der Waals interaction between both the backbones. The synthesized hydrogel also depicted a reduction in the intensity of peak or crystallinity (Fig. S1d†), which may be due to the intermolecular hydrogen bonding and electrostatic interactions between the functional group of acrylic acid, cellulose, and gelatin.[40,43]

3.3. Characterization of AgNPs

3.3.1. UV-visible studies. AgNPs have the unique optical property that they interfere with light and lead to the SPR band in the UV-visible spectrum. The type and arrangement of the SPR band depended on the particle size, their shape, and the aggregation of AgNPs.[44] The SPR band was found at 416 nm, which depicted the spherical synthesis of AgNPs[45] (Fig. 5a). The synthesized AgNPs was then evaluated with a diverse concentration of $AgNO_3$ (0.002 M–0.01 M). As the concentration of AgNPs increased, there was an enhancement in the intensity of the adsorption band. The UV spectra of AgNPs at different pH in the range of 6–12 was studied (Fig. 5b). It was clear from the result that with the increase in pH, the adsorption intensity was

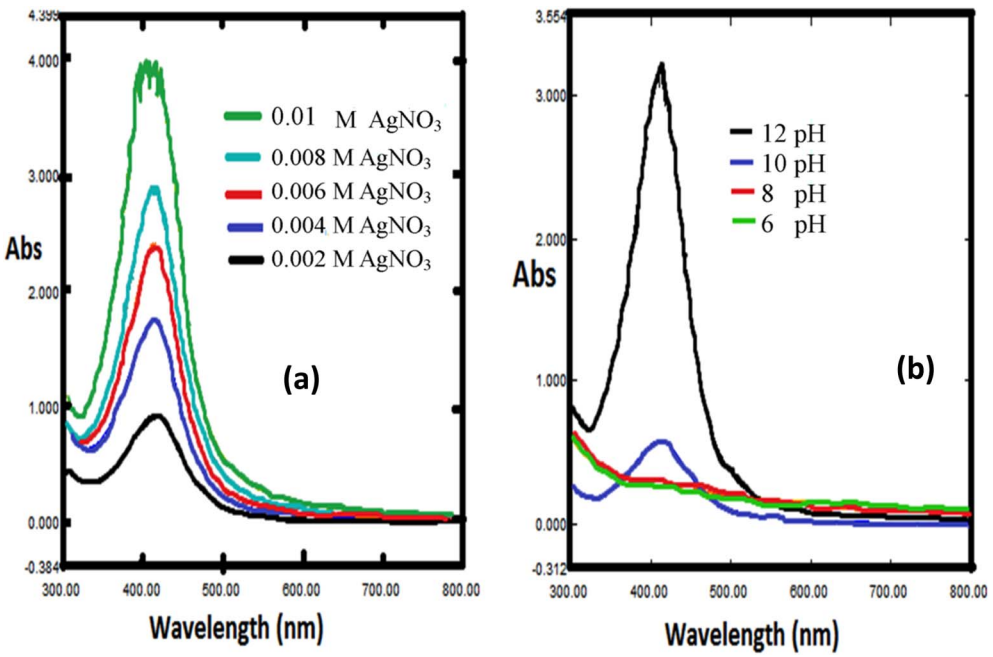

Fig. 5 UV-visible absorption spectra of AgNPs at different concentrations of (a) $AgNO_3$ and (b) pH.

also increased. This may be due to the fact that at higher pH, there is an increase in the ionization of the functional groups of the synthesized hydrogel and this leads to the reduction of silver ions.[43,46] The optimized conditions for the synthesis of AgNPs by C-G-poly(AA) occurred with the SPR band at 416 nm and pH 12 with $AgNO_3$ concentration of 0.01 M (Fig. 5a), but at a concentration of 0.01 M, the UV spectra showed disturbance. Thus, for further work, 0.08 M concentration of silver nitrate was used instead of 0.01 M.

3.3.2. XRD analysis. Synthesized AgNPs was stabilized with C-G-poly(AA). The nature of the prepared AgNPs was studied through XRD and the result depicted the crystalline nature of AgNPs (Fig. 6a) with four Bragg's reflections (110), (201), (222), and (310) at 2θ angles of 37.46°, 43.32°, 63.42°, and 76.42°, respectively. The reflections confirmed the fcc structure of metallic silver. The lattice parameter determined from the XRD pattern was 4.08329 Å. The size of the AgNPs was calculated by the Debye–Scherrer equation.[43,44,47]

$$d = \frac{k\lambda}{\beta\cos\theta}$$

The FWHM for AgNPs was 0.70 at 44.58°, and the average particle size was 11.89 nm. The XRD of synthesized C-G-g-poly(AA) is given in Fig. 6b. The result of C-G-poly(AA) showed a broad peak at 2θ angle of 22°, which showed the amorphous nature of the synthesized C-G-poly(AA).[43,45] The sharp peaks at the 2θ angles of 39°, 44°, 67°, and 79° confirm the presence of AgNPs in the C-G-g-poly(AA).

3.3.3. Energy dispersive X-ray spectroscopy (EDS), transmission electron microscopy (TEM), selected-area electron diffraction (SAED) pattern, and zeta potential of silver nanoparticles. The EDS result (Fig. 7a) showed a spectral line near 3 keV, which strongly shows the silver region and thus gave a clear-cut indication of the formation of silver nanoparticles. The results clearly showed that silver is the major constituent in the sample. The presence of copper and carbon signals in the EDS are due to the coating of the sample in the copper grid aircraft. The size and morphology of the synthesized AgNPs was studied through TEM. The TEM and SAED results (Fig. 7b and c) showed that AgNPs are formed in the nanometer range and are spherical shape. The average diameter of the synthesized AgNPs was in the range of 11–25 nm. The average size calculated from XRD was in conformity with the TEM and SAED. The SAED pattern (Fig. 7c) illustrated different rings with spots, which confirmed the fcc crystalline structure of AgNPs. The SAED pattern indicated the polycrystalline nature of the synthesized AgNPs.[48–50] The zeta potential technique was utilized to study the surface charge and stability of AgNPs in the solution (Fig. 7d). The zeta potential value for the synthesized silver nanoparticles by C-G-g-poly(AA) was found to be +49.2 mV, which means that there is a net positive charge on the AgNPs and it was stable in the aqueous solution.[51]

3.4. Stability of synthesized AgNPs

Synthesized silver nanoparticles were stored for 6 months and their stability was checked by TEM (Fig. S2†), which revealed well-dispersed AgNPs without any variation in their size and morphology. Thus, this confirms that the C-G-g-poly(AA) hydrogel acts as a stabilizing agent for silver nanoparticles.

3.5. Catalytic evaluation of synthesized AgNPs for dye degradation

The use of synthetic dyes increase every year in different industries such as paper, textile, cosmetic, and food sectors. These

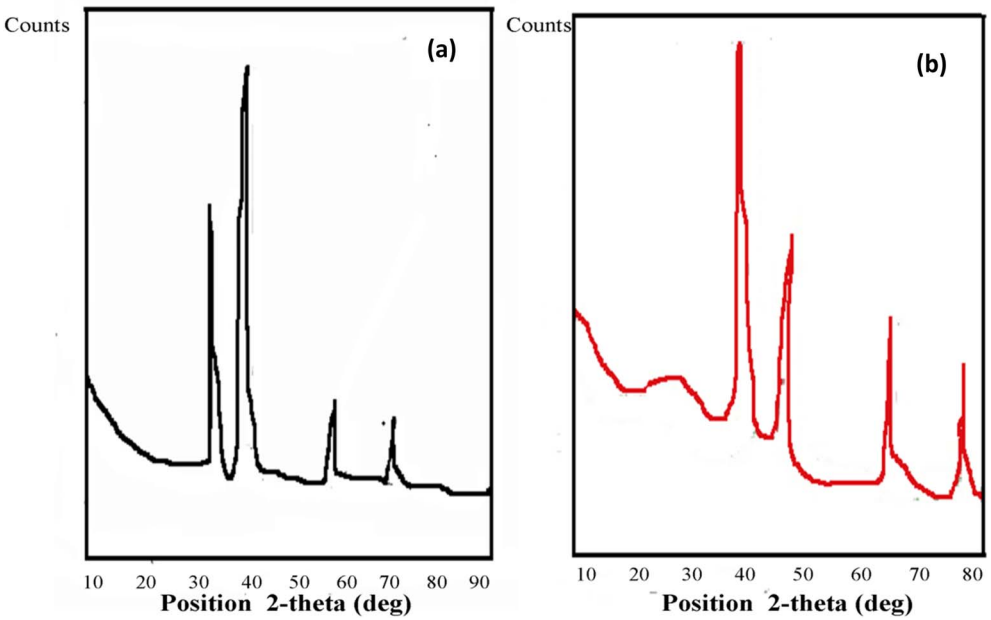

Fig. 6 X-ray diffraction pattern of AgNPs synthesized by (a) C-G-g-poly(AA) and (b) C-G-g-poly(AA)-AgNPs.

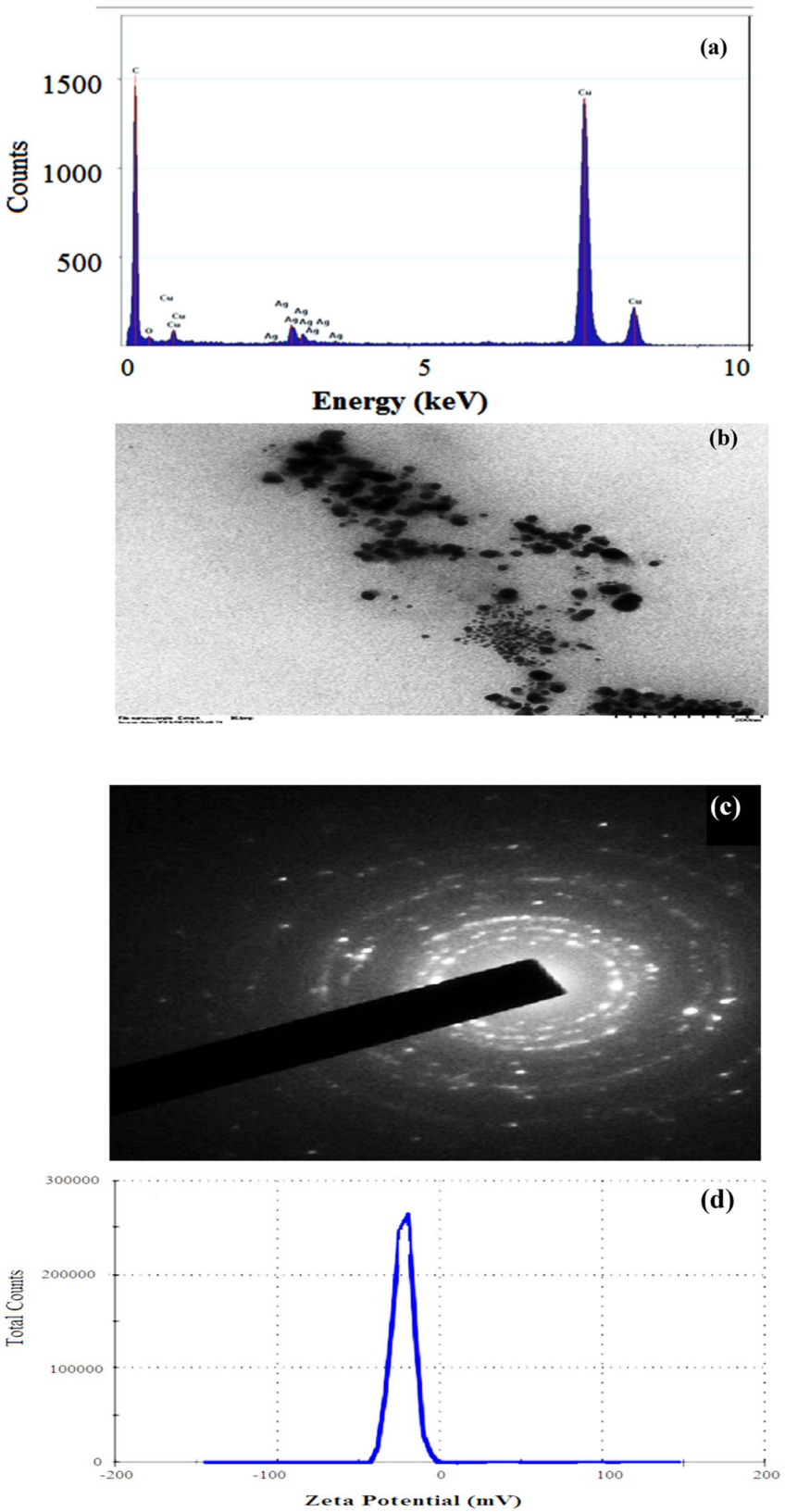

Fig. 7 Characterization of AgNPs using (a) EDS, (b) TEM, (c) SAED pattern, and (d) zeta potential synthesized with C-G-g-Poly(AA).

dyes are toxic, stable in nature, and are difficult to degrade and reduce naturally. A large amount of dye waste is discharged into the water system every day. These wastes are a serious threat to our ecosystem and major concern to the researchers. Many catalysts are used, which convert these xenobiotic dyes into a nontoxic component, which are easily biodegradable in nature.[52–54] The synthesized C-G-g-poly(AA) AgNPs was used as a catalyst for the reduction of ethidium bromide and eosin dye using sodium borohydride as a reductant. The reduction and degradation mechanism of both the dyes, ethidium bromide and eosin, in the presence of $NaBH_4$ and C-G-g-poly(AA)-AgNPs is given in Scheme 2. The UV-vis absorption spectra showed the dye reduction/degradation reaction with $NaBH_4$ in the presence and absence of the synthesized hybrid AgNPs hydrogel. Dye degradation in the absence of C-G-g-poly(AA)-AgNPs was used as a blank in the experiment. The results of EtBr reduction through a UV-vis spectrophotometer clearly showed that reduction and degradation occurred by sodium borohydride reductant. The reduction was faster when synthesized silver nanoparticles were used with sodium borohydride. The adsorption maxima for eosin dye was found at 517 nm. The dye reduction results of eosin showed that in the absence of AgNPs, the dye was degraded within 27 min, and in the presence of AgNPs (Fig. 8a), only 6 min were required to degrade eosin dye (Fig. 8b). The λ_{max} of EtBr was 480 nm. EtBr degradation results showed that it was degraded in 18 min (Fig. 9a) in the absence of AgNPs and only 4 min were required to completely degrade it in the presence of AgNPs and sodium borohydride (Fig. 9b). AgNPs acted as an electron transmitter and started transferring the electron from the BH_4^- ion (donor B_2H_4/BH_4^-) to the acceptor (organic dye), which leads to dye reduction. The BH_4^- ion is adsorbed onto the AgNPs surface and this transfers the electron from the BH_4^- ion to the dye by AgNPs. Thus, the results clearly depicted that EtBr degradation was faster and effective in the presence of AgNPs. Higher dye reduction/degradation rate in the presence of nanoparticles may be due to the presence of a larger surface area for the reactant in the reduction process.[55–57] There are many carboxyl groups present in the surface of the polymer chain of PAA, which can bind with the AgNPs and make the AgNPs water-soluble and stable. Thus, these water soluble and stable silver nanoparticles will have high efficiency in the reduction of dyes.[58,59]

The dye concentration used for the degradation process is 0.08 M and the $NaBH_4$ concentration used for the degradation process was 0.1 M. The reduction process followed the pseudo first order kinetics and it was calculated using the equation given below[50,60–64]

$$\ln\left(\frac{A_t}{A_0}\right) = -kt$$

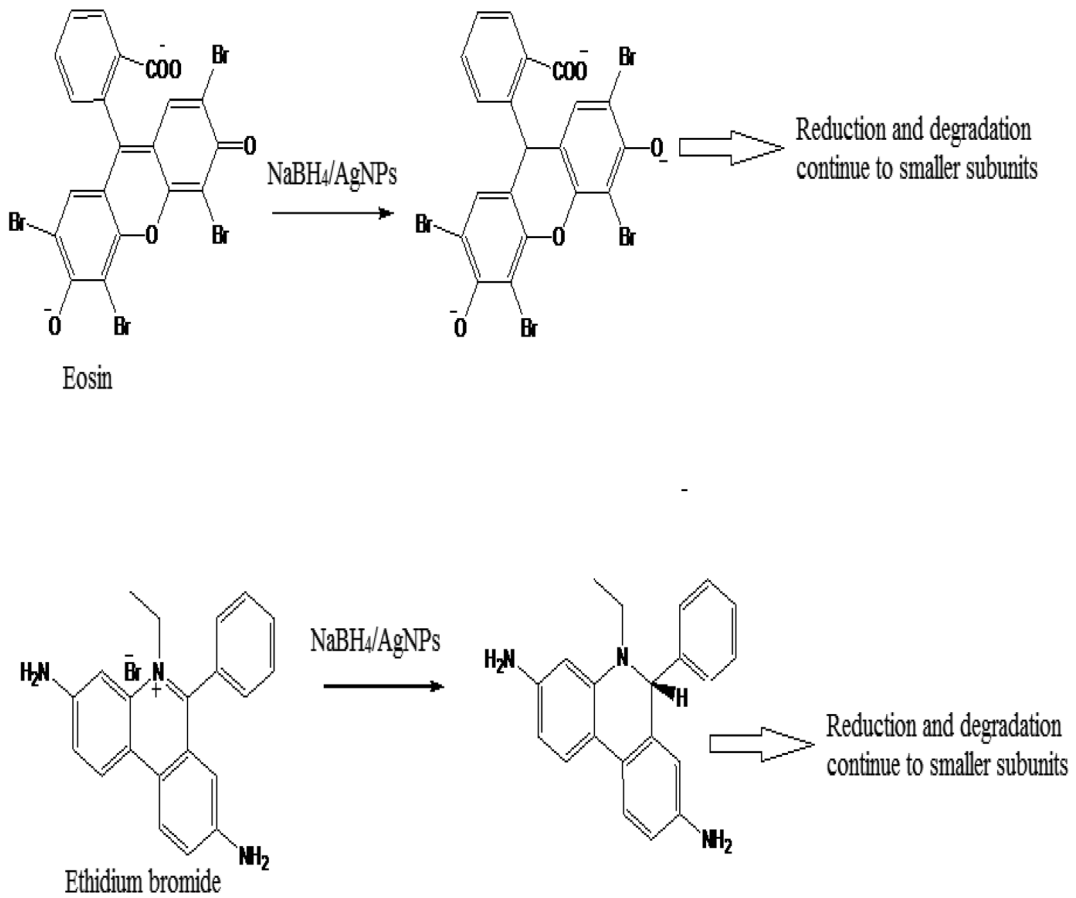

Scheme 2 Eosin and ethidium bromide dye reduction/degradation in the presence of $NaBH_4$ and C-G-g-poly (AA)-AgNPs.

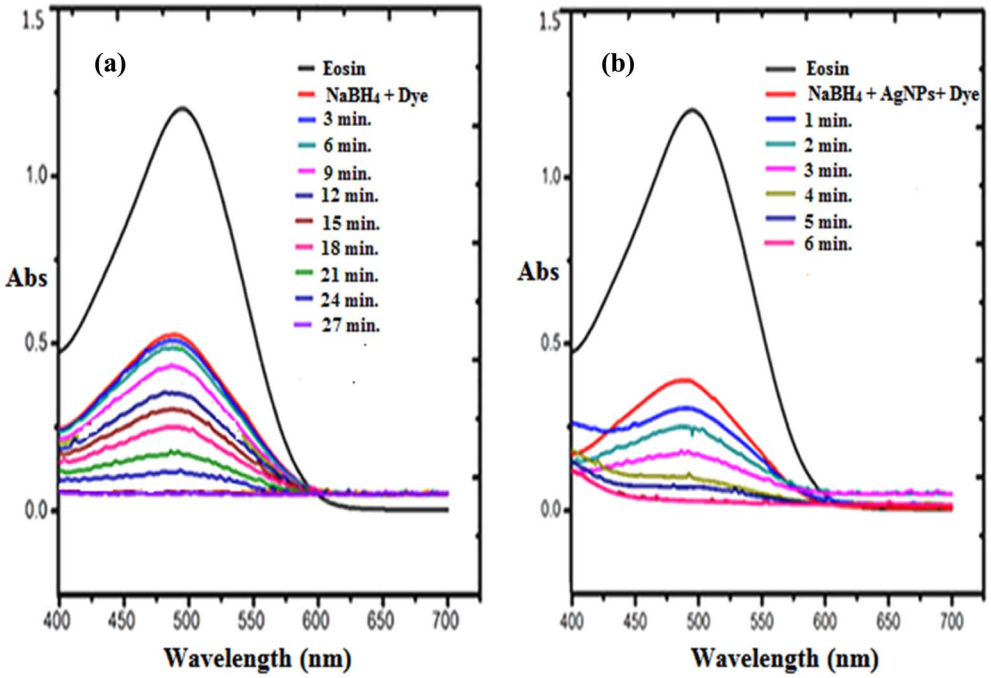

Fig. 8 UV-visible spectra for the degradation of eosin dye in the presence of (a) $NaBH_4$ and (b) in the presence of $NaBH_4$ and C-G-g-poly(AA)-AgNPs.

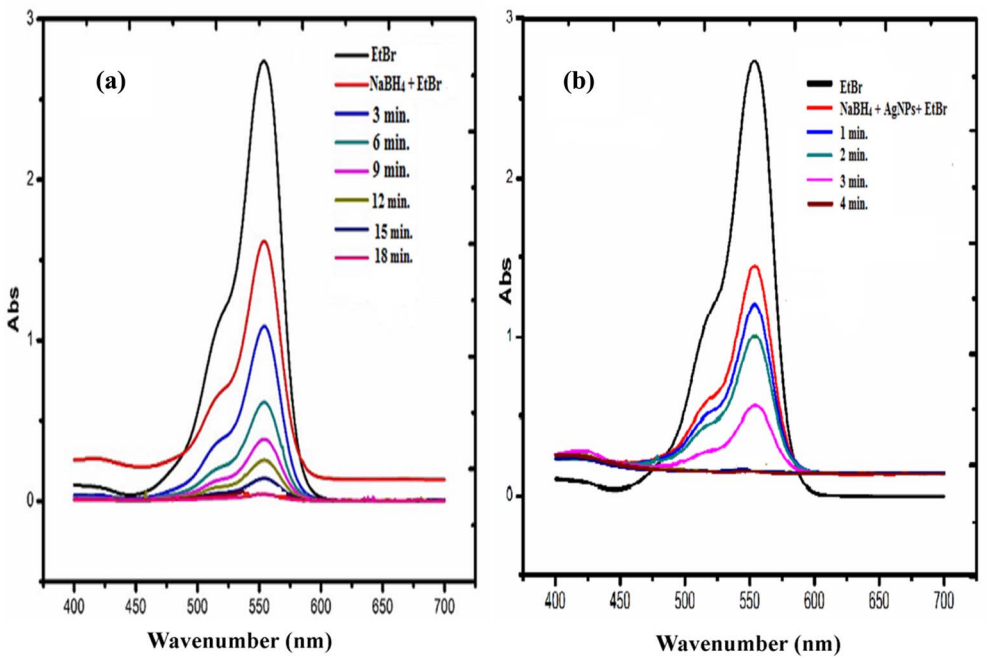

Fig. 9 UV-visible spectra for the degradation of ethidium bromide dye in the presence of (a) $NaBH_4$ and (b) in the presence of $NaBH_4$ and C-G-g-poly(AA)-AgNPs.

where k and t are the 1st order rate constant (s^{-1}) and reaction time, respectively, while A_t and A_0 are the dye absorbance at time t and 0, respectively.

The absorbance of EtBr (Fig. S3a and b†) and eosin (Fig. S3c and d†) dyes were studied with respect to time and in the presence and absence of C-G-g-poly(AA)-AgNPs hydrogel. The rate constants for both the dyes are given in Table 1. The results clearly indicated that the rate constants were higher in EtBr and eosin (Table 1) with the use of C-G-g-poly(AA)-AgNPs, which was in agreement with the literature data.[44,65,66] Thus, it can be

Table 1 Rate constants for the reduction of dyes by $NaBH_4$ in the presence and absence of C-G-g-poly(AA)-AgNPs

Dyes	k (sec^{-1}) in the absence of C-G-g-poly (AA)AgNPs	k (sec^{-1}) in the presence of C-G-g-poly (AA)AgNPs
Ethidium bromide	0.0014	0.0093
Eosin	0.0023	0.0059

concluded that AgNPs-imbibed hydrogel acts as a very effective catalyst for the degradation of EtBr and eosin dye.

4. Conclusion

The above discussion showed the successful synthesis of a novel C-G-g poly(AA)-AgNPs hydrogel through grafting and cross-linking. The synthesized AgNPs-imbibed hydrogel is mechanically and thermally more stable than cellulose and gelatin. The AgNPs synthesized were spherical with a size range of 11–30 nm. The synthesized hydrogel has very good swelling capacity, and the maximum swelling ratio was found to be 92 g g^{-1}. The C-G-poly(AA)-AgNPs formed acted as a very effective catalyst for the reduction and degradation of the carcinogenic dyes EtBr and eosin. EtBr and eosin dye degradation rate was more than 4 times faster when AgNPs were used with sodium borohydride. Thus, it can be concluded that the synthesized C-G-g- poly(AA)-AgNPs hybrid hydrogel is efficient for the reduction and degradation of the carcinogenic dyes EtBr and eosin.

Conflicts of interest

There is no conflict of interest for this manuscript.

Acknowledgements

Authors Saruchi and Vaneet Kumar are thankful to CT Group of institutions for providing facility to carry out this research work. The authors are grateful to the Researchers Supporting Project number (RSP2023R407), King Saud University, Riyadh, Saudi Arabia, for the financial support.

References

1 E. Abbasi, M. Milani, S. F. Aval, M. Kouhi, A. Akbarzadeh, T. H. Nasrabadi, P. Nikasa, S. W. Joo, Y. Hanifehpour, K. Nejati-Koshki and M. Samiei, *Critic. Rev. Microbiol.*, 2016, **42**, 173–180.
2 E. S. Abdel-Halim and S. S. Al-Deyab, *Carbohydr. Polym.*, 2011, **86**, 1615–1622.
3 D. N. Ahmed, L. A. Naji, A. A. H. Faisal, N. Al-Ansari and M. Naushad, *Sci. Rep.*, 2020, **10**, 2042, DOI: **10.1038/s41598-020-58866-y**.
4 N. N. Bonia, M. S. Kamaruddin, M. H. Nawawi, S. Ratim, H. N. Azlina and E. S. Ali, *Procedia Chem.*, 2016, **19**, 594–602.
5 R. Bryaskova, N. Georgieva, D. Pencheva, Z. Todorova, N. Lazarova and T. Kantardjiev, *Colloids Surf., A*, 2014, **444**, 114–119.
6 H. Chen, S. Zhang, A. Zhao, M. Liu and Q. Zhang, *Prog. Chem.*, 2019, **31**, 5571–5579.
7 J. P. Cook, G. W. Goodall, O. V. Khutoryanskaya and V. V. Khutoryankiy, *Macromol. Rapid Commun.*, 2012, **33**, 332–336.
8 R. Dash, M. Foston and A. J. Ragauskas, *Carbohydr. Polym.*, 2013, **91**, 638–645.
9 V. Dhand, L. Soumya, S. Bharadwaj, S. Chakra, D. Bhatt and B. Sreedhar, *Mater. Sci. Eng., C*, 2016, **58**, 36–43.
10 M. Eid, M. A. Abdel-Ghaffar and A. M. Dessouki, *Phys. Res. B Nucl. Instrum. Meth. B.*, 2009, **267**, 91–98.
11 W. H. Eisa, A. M. Abdelgawad and O. J. Rojas, *ACS Sustainable Chem. Eng.*, 2018, **6**, 1–37.
12 A. A. H. Faisal, S. F. A. Al-Wakel, H. A. Assi, L. A. Naji and M. Naushad, *J. Water Process Eng.*, 2020, **33**, 101112, DOI: **10.1016/j.jwpe.2019.101112**.
13 J. Ge, Y. Hu, M. Biasini, C. Dong, J. Guo, W. P. Beyermann and Y. Yin, *Chem.–Eur. J.*, 2007, **13**, 7153.
14 J. P. Gong, Y. Katsuyama, T. Kurokawa and Y. Osads, *Adv. Mater.*, 2003, **15**, 1155–1158.
15 Y. X. Hu, J. P. Ge, D. Lim, T. Zhang and Y. D. Yin, *J. Solid State Chem.*, 2008, **181**, 1524–1529.
16 W. H. W. Ishak, I. Ahmad, S. Ramli and M. C. I. M. Amin, *Nanomaterials*, 2018, **8**, 749–761.
17 S. Joseph and B. Mathew, *Mater. Sci. Eng. B*, 2015, **195**, 90–97.
18 B. S. Kaith, K. Sharma, V. Kumar, S. Kalia and H. C. Swart, *Synth. Met.*, 2014, **187**, 61–67.
19 B. S. Kaith, Saruchi, R. Jindal and M. S. Bhatti, *Soft Matter*, 2012, **8**, 2286–2293.
20 M. Kaushik and A. Moores, *Green Chem.*, 2016, **18**, 622–637.
21 T. Klaus-Joerger, R. Joerger, E. Olsson and C. G. Granqvist, *Trends Biotechnol.*, 2001, **19**, 15–20.
22 A. Kljun, A. S. Thomas, S. Benians, F. Goubet, F. Meulewaeter, J. P. Knox and R. S. Blackburn, *Biomacromolecules*, 2011, **12**, 4121–4126.
23 X. T. Le, L. E. Rioux and S. L. Turgeo, *Adv. Colloid Interface Sci.*, 2017, **239**, 127–135.
24 G. Li, Y. Li, Z. Wang and H. Liu, *Mater. Chem. Phys.*, 2017, **187**, 133–140.
25 J. Liang, F. Zeng, M. Zhang, Z. Pan, Y. Chen, Y. Zeng, Y. Xu, Q. Xu and Y. Huang, *RSC Adv.*, 2015, **54**, 42990–43905.
26 B. Mandal and S. K. Ray, *Mater. Sci. Eng., C*, 2014, **44**, 132–143.
27 B. Mandal B and S. K. Ray, *J. Taiwan Inst. Chem. Eng.*, 2016, **60**, 313–327.
28 H. Mittal, V. Kumar, Saruchi and S. S. Ray, *Int. J. Biol. Macromol.*, 2016, **89**, 1–11.
29 M. Naushad, Z. A. ALOthman, M. R. Awual, M. M. Alam and G. E. Eldesoky, *Ionics*, 2015, **21**, 2237–2245, DOI: **10.1007/s11581-015-1401-7**.
30 M. Naushad, *J. Chem. Eng.*, 2014, **235**, 100–108, DOI: **10.1016/J.CEJ.2013.09.013**.
31 M. Naushad, G. Sharma and Z. A. Alothman, *J. Cleaner Prod.*, 2019, **241**, 118263.

32 M. D. Onofrei and A. Filimon, Cellulose-based hydrogels: designing concepts, properties, and perspectives for biomedical and environmental applications, in *Polymer science: research advances, practical applications and educational aspects*, ed. A. Mendez-Vilas and A. Solano-Martin, Formatex Research Center Publication, Spain, 2016, pp. 108–120, ISBN: 978-84-942134-8-9.
33 Saruchi, B. S. Kaith, R. Jindal and V. Kumar, *Polym. Degrad. Stab.*, 2015, **115**, 24–31.
34 Saruchi, B. S. Kaith, R. Jindal, V. Kumar and M. S. Bhatti, *RSC Adv.*, 2014, **4**, 39822–39829.
35 M. L. Oyen, *Int. Mater. Rev.*, 2014, **59**, 44–59.
36 Z. Parang, A. Keshavarz, S. Farahi, S. M. Elahi, M. Ghoranneviss and S. Parhoodeh, *Sci. Iran.*, 2012, **19**, 943–947.
37 G. M. Raghavendra, J. Jung, D. Kim and J. Seo, *Int. J. Biol. Macromol.*, 2016, **86**, 126–128.
38 G. V. N. Rathna, D. V. M. Rao and P. R. Chatterji, *J. Macromol. Sci., Part A: Pure Appl.Chem.*, 1996, **33**, 1199–1207.
39 P. Rokhade, S. A. Agnihotri, S. A. Patil, N. N. Mallikarjuna, P. V. Kulkarni and T. M. Aminabhavi, *Carbohydr. Polym.*, 2006, **65**, 243–252.
40 Saruchi, B. S. Kaith, V. Kumar and R. Jindal, *Biotechnol. Rep.*, 2016, **9**, 74–81.
41 V. K. Saruchi, *Arabian J. Chem.*, 2019, **12**, 316–329.
42 S. Senapati, *Biosynthesis and immobilization of nanoparticles and their applications*, PhD Thesis, University of pune, India, 2005, vol. 1–57.
43 K. Sharma, B. S. Kaith, V. Kumar, S. Som, S. Kalia and H. C. Swart, *RSC Adv.*, 2013, **48**, 25425–26482.
44 W. Song, P. Ge, Q. Ke, Y. Sun, F. Chen, H. Wang, Y. Shi, X. Wu, H. Lin, J. Chen and C. Shen, *Chemosphere*, 2019, **221**, 166–174.
45 M. Tally and Y. Atassi, *J. Polym. Res.*, 2015, **22**(9), 1–13.
46 S. Tang, N. Li, D. Yuan, J. Tang, X. Li, C. Zhang and Y. Rao, *Chemosphere*, 2019, **234**, 658–667.
47 V. Thivaharan, S. Raja and R. Vinayagam, *J. Mol. Liq.*, 2016, **221**, 1063–1070.
48 Q. H. Tran, V. Q. Nguyen and A. T. Le, *Nanosci. Nanotechnol.*, 2013, **4**, 1–20.
49 W. Treesuppharat, P. Rojanapanthu, C. Siangsanoh, H. Manuspiy and S. Ummartyotin, *Biotechnol. Rep.*, 2017, **15**, 84–91.
50 P. Vasileva, B. Donkova, I. Karadjova and C. Dushkin, *Colloids Surf., A*, 2011, **382**, 203–210.
51 J. Venkatesan, J. Y. Lee, D. S. Kang, S. Anil, S. K. Kim, M. S. Shim and D. G. Kim, *Int. J. Biol. Macromol.*, 2017, **98**, 515–525.
52 M. Venkatesham, D. Ayodhya, A. Madhusudhan, N. V. Babu and G. Veerabhadram, *Appl. Nanosci.*, 2014, **4**, 113–119.
53 K. Vimala, K. S. Sivudu, Y. M. Mohan, B. Sreedhar and K. M. Raju, *Carbohydr. Polym.*, 2009, **75**, 463–471.
54 W. B. Wang, D. Huang, Y. Kang and Ai-Qi. Wang, *Colloids Surf., B*, 2013, **106**, 51–59.
55 L. Wei, J. Lu, H. Xu, A. Patel, Z. Chen and G. Chen, *Drug Discovery*, 2015, **20**, 595–601.
56 X. L. Wu, Y. Shi, S. Zhong, H. Lin and J. R. Chen, *Appl. Surf. Sci.*, 2016, **378**, 80–86.
57 X. L. Wu, Y. Shi, S. Zhong, H. Lin and J. R. Chen, *Appl. Surf. Sci.*, 2016, **378**, 80–86.
58 B. Xia, Q. Cui, F. He and L. Li, *Langmuir*, 2012, **28**, 11188–11194.
59 P. Xiao, J. Lou, H. Zhang, W. Song, X. L. Wu, H. Lin, J. Chen, S. Liu and X. Wang, *Catal. Sci. Technol.*, 2018, **8**, 201–209.
60 M. S. Yakout and A. A. Mostafa, *Int. J. Clin. Exp. Med.*, 2015, **8**, 3538–3544.
61 M. Zhang, N. S. Yang, N. G. Portney, D. Cui, G. Budak, E. Ozbay, M. Ozkan and C. S. Ozkan, *Biomed. Microdevices*, 2008, **10**, 321–328.
62 Q. Zhang, Q. Yang, P. Phanlavong, Y. Li, Z. Wanga, T. Jiao and Q. Peng, *ACS Sustainable Chem. Eng.*, 2017, **5**, 4161–4170.
63 Saruchi, V. Kumar and B. S. Kaith, *Ind. Eng. Chem. Res.*, 2016, **55**, 10492–10499.
64 Saruchi, V. Kumar, V. Rehani and B. S. Kaith, *Iran. Polym. J.*, 2018, **27**, 913–926.
65 C. Zhou, Q. Wua, Y. Yue and Q. Zhang, *J. Colloid Interface Sci.*, 2011, **353**, 116–123.
66 Y. Zhou, S. Fu, L. Zhang and H. Zhan, *Carbohydr. Polym.*, 2013, **97**(2), 429–435.